PHYSICS RESULTS FROM THE CERN PROTON-ANTIPROTON COLLIDER

J. D. Dowell

Department of Physics, University of Birmingham, England

الخلاصة :

نقدم نتائج من تشغيل (١٩٨١ — ١٩٨٢) الصادم CERN للبروتون — مضاد برتون عند طاقة ٥٤٠ بليون إلكترون فولت من تجارب UA1, UA2, UA4, UA5. المقطع العرضي الكلي يساوي ٦٦±٧ ميللي بارن يبين الإرتفاع المتوقع عند الطاقات المنخفضة . قياسات التشتت المرن متوافقة مع لوغاريثم الإنكماش للقمة الأمامية .

الكثافة المركزية للتسارع الزائف للإنتاج الشامل للجسيمات المشحونة يرتفع لوغاريثمياً حتى يصل إلى قيمة ٣,٣ جسيماً لكل وحدة تسارع . وتوزيع التعدد يظهر مقياس KNO عندما يقارن بنتائج ISR تحت ٦٣ بليون إلكترون فولت وأيضاً تعطى نتائج عن الفوتون الشامل والجسيمات الغريبة وإنتاج الفوتون .

ولقد وجد أن طيف P_t للجسيم الواحد مسطح لحد بعيد لقيم P_t حتى ١٠ بليون إلكترون فولت/سرعة الضوء وذلك أكثر من القيمة لـ ISR وتبين أيضاً أنه يعتمد على التعدد .

كما أننا نعطي دليلاً على النفث . كلا النفث ومقطع الجسيم الواحد يتفق مع تنبؤ QCD عند قيم عالية من P_t ونعطي تقرير نتائج سلبية في البحث عن سنترو (Centauro) وكواركس (Quarks) الحرة .

وأخيراً نقدم دليلاً عن البوزون المتوسط الضعيف (Weak Intermediate Bosom) الذي حصل عليه من تجارب UA1, UA2.

0377-9211/83/040301-16$01.60

ABSTRACT

Results from the 1981 and 1982 operation of the CERN $p\bar{p}$ collider at 540 GeV obtained in experiments UA1, UA2, UA4, and UA5 are presented. The total cross section of 66 ± 7 mb shows the expected rise from lower energies. Elastic scattering measurements are consistent with a $\ln s$ shrinkage of the forward peak. The central pseudo-rapidity density for inclusive charged particle production rises as $\ln s$ reaching a value of 3.3 particles per unit of rapidity and the multiplicity distribution exhibits KNO scaling when compared to ISR results below 63 GeV. Results for inclusive photon, strange particle, and proton production are also given. The single particle p_t-spectrum for p_t up to 10 GeV/c is considerably flatter than at the ISR and shows a dependence on multiplicity. Evidence for jets is given. Both jet and single particle cross sections at high p_t agree with QCD predictions. Negative searches for Centauro events and free quarks are reported. Finally the evidence for the Weak Intermediate Boson, W, obtained in the UA1 and UA2 experiments, is presented.

PHYSICS RESULTS FROM THE CERN PROTON–ANTIPROTON COLLIDER

1. INTRODUCTION

The proton–antiproton collider was suggested in 1976 by C. Rubbia and co-workers [1] and came into operation in July 1981. The decision to build it was made in 1978 after the success of the Initial Cooling Experiment (ICE) [2] that demonstrated the feasibility of accumulating antiprotons in sufficient quantities, reducing their phase space by stochastic cooling—a technique first studied by S. Van der Meer in 1968 [3]. Construction of the Antiproton Accumulator (AA) started in 1978 [4] and five experiments to use the collider were approved in the middle of the year. The modifications to the SPS, the construction of the AA and of the experiments were all accomplished in a remarkably short time.

The availability of 540 GeV in the center of mass makes possible for the first time the observation of the weak intermediate bosons $W^{\pm}$ and Z^0. The design luminosity of $10^{30}\,cm^{-2}\,s^{-1}$ has not yet been reached but luminosities approaching $10^{29}\,cm^{-2}\,s^{-1}$ have been achieved in 1983 with regular operation at $5\times10^{28}\,cm^{-2}\,s^{-1}$ with a lifetime of $\sim$20 hrs. This produces typically 1 $W^{\pm}$ per day decaying leptonically in the largest experiment UA1, and theoretically 1 Z^0 every ten days. Data obtained up to the end of 1982 have been analyzed and are discussed here. Early running in October–December 1981 was at a typical luminosity of $\sim3\times10^{26}\,cm^{-2}\,s^{-1}$ but allowed a first look at strong interaction physics at ten times the accelerator energy previously available, with an integrated luminosity of $\sim2\times10^{32}\,cm^{-2}$, too low to have seen a W but good enough to search for interesting phenomena seen so far only with cosmic rays. Improvements in reliability and beam handling resulted in luminosities of a few $\times\,10^{28}\,cm^{-2}\,s^{-1}$ in October–December 1982 and produced the first handful of W events. Results from UA1, UA2, UA4, and UA5 will be discussed.

Antiprotons have also been stored in the ISR and several groups have reported results [5]. Their main impact has been to show that $p\bar{p}$ and pp interactions are very similar at this relatively high energy ($\sqrt{s}=53$ GeV) apart from a few expected differences that arise from the different charges and baryon numbers of the incident particles. The main interest therefore is to compare $p\bar{p}$ interactions at the much higher energy of 540 GeV with pp results from the ISR up to $\sqrt{s}=63$ GeV in order to study energy dependent effects and to extend the range of transverse momentum available.

2. THE UA EXPERIMENTS

The UA1 detector [6] (Figure 1) was designed as a general purpose instrument with an almost 4π solid angle coverage extending down to polar angles of a few mrad. Its central part is a 6 m long, 2.4 m diameter drift chamber system with 18 cm drift spaces. The image readout gives space points at centimeter intervals along the tracks and records ionization information. The central track detector is surrounded along its length by 48 semicylindrical electromagnetic calorimeters and at each end by 32 similar radial sectors. All of the above are inside the coil of a dipole magnet (7 m × 3.5 m × 3.5 m) which produces a highly uniform field of 0.7 T. The laminated return yoke of the magnet, equipped with scintillation counters, also serves as a hadron calorimeter. The outer shell of the detector is a large-area muon detector consisting of 8 layers of drift tubes (2 separated chambers each with 4 layers). Calorimeterized compensator magnets, small angle calorimeters and further track detectors extend the detection to angles less than 5°. The measured rms accuracy of the central drift chambers is 280 μm giving a transverse momentum resolution $\Delta p_t/p_t\sim0.02p_t$. The electromagnetic and hadron calorimeters have energy resolutions $\Delta E/E$ of $0.15/\sqrt{E}$ and $0.8/\sqrt{E}$ respectively. An independent means of measuring the luminosity is provided by small drift chambers at $\pm$22 m to measure elastic scattering by detecting collinear particles.

The UA2 detector [7] (Figure 2), well matched to the $W^{\pm}$, Z^0 search, is composed of finely segmented calorimeter cells, 240 in the central region and 240 in the forward and backward cones. They are arranged in tower structures pointing at the intersection region. An inner detector, using drift and proportional chambers, determines the vertex position. The forward and backward detectors include magnetic spectrometers (toroidal magnets and drift chambers) to measure the asymmetry of the electrons from $W^{\pm}$ decays. For the 1981 and 1982 runs a 60° azimuthal wedge of the central calorimeter is replaced by a magnetic spectrometer covering ±0.7 units of rapidity which

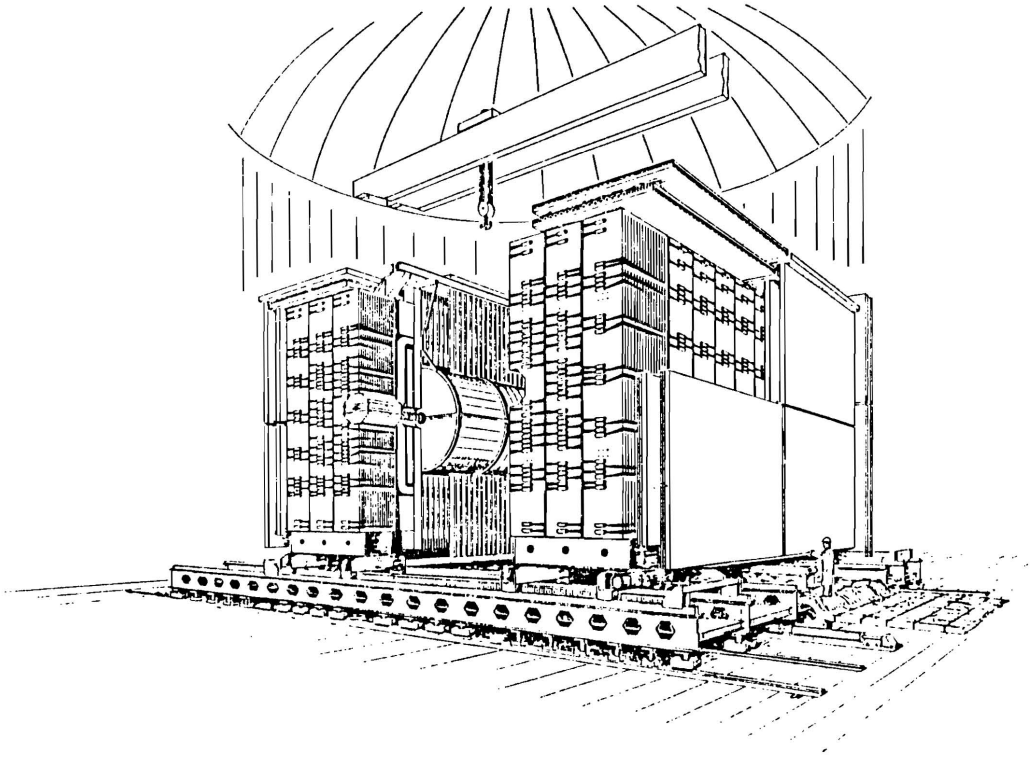

Figure 1. View of the Central Part of the UA1 Detector

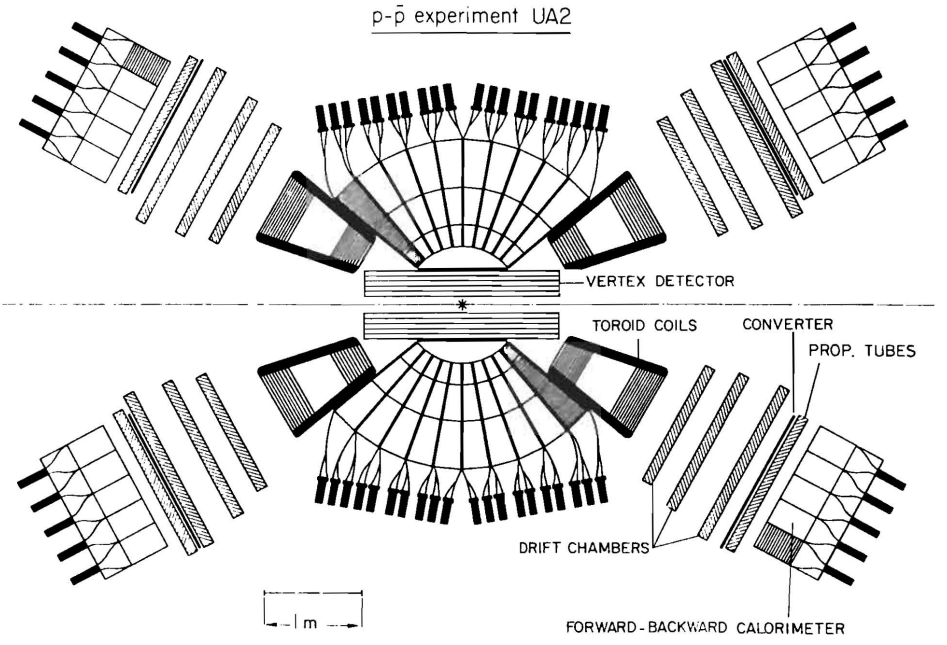

Figure 2. Plan View of the UA2 Experiment

uses drift chambers, time of flight counters and a lead-glass array, outside the main apparatus, that can be used to identify charged particles and neutral pions.

Experiment UA3 [8] shares the same intersection region as UA1 and is a search for magnetic monopoles by looking for their expected high ionization in 125 μm thick kapton foils. These are placed both inside and outside the vacuum chamber near the intersection point and around the outside of the UA1 central track detector. The foils have been scanned but no evidence for monopoles has yet been observed.

Experiment UA4 [9] coexists with UA2. It measures elastic scattering and (using the optical theorem) the $p\bar{p}$ total cross section. Small drift and proportional chambers can be placed very near to the beams inside 'Roman pots' situated 40 m on either side of the intersection point. Smaller angles of scattering can be detected than in UA1.

The main part of the UA5 detector [10] consists of two 6 m long streamer chambers above and below the intersection region incorporating lead-glass plates to allow photon detection. There is no magnetic field and the experiment is an alternative to UA2. It is designed to study simple characteristics of particle production. (See Figure 3.)

As data acquisition rates are limited some form of triggering is needed to select events of interest. Up to now, two types of trigger have been used to study inelastic events: (*a*) simple hodoscopes at each end of the detector (UA1, UA2, UA5) giving a 'minimum bias' trigger and (*b*) transverse energy triggers (UA1, UA2) where $E_T = \Sigma E_i \sin\theta_i$ is summed over calorimeter cells and a threshold is imposed to select high p_t processes.

3. ELASTIC SCATTERING AND TOTAL CROSS SECTION

$p\bar{p}$ elastic scattering has been measured by UA4 [11] and UA1 [12] in two adjacent ranges of $-t$ centered at 0.1 $(\text{GeV}/c)^2$ and 0.2 $(\text{GeV}/c)^2$ giving different exponential slope parameters b of 17.2 ± 1.0 $(\text{GeV}/c)^{-2}$ and 13.3 ± 1.5 $(\text{GeV}/c)^{-2}$ respectively where $dN_{el}/dt \propto \exp(bt)$ (see Figure 4). Both slopes agree with extrapolations from ISR energies and are consistent with a logarithmic ($\ln s$) shrinkage with increasing energy of the width of the forward elastic differential cross section peak as expected from Pomeron exchange with a nonzero Regge-trajectory slope [13]. The total cross section σ_t is obtained from

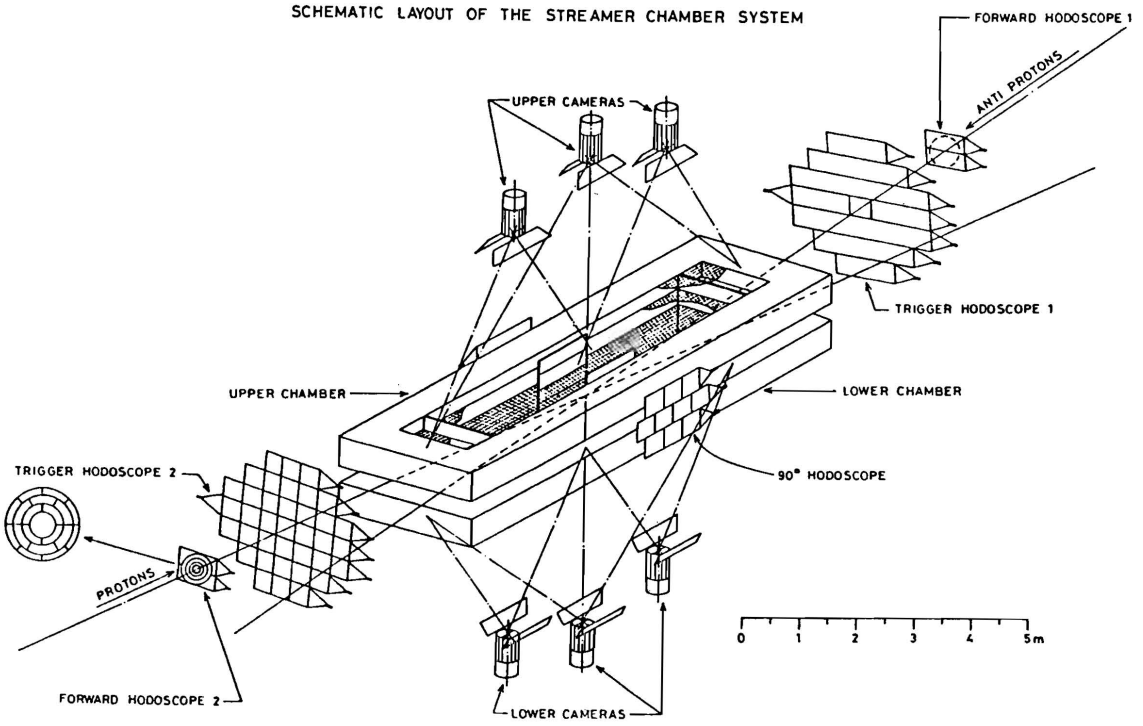

Figure 3. The UA5 Experiment

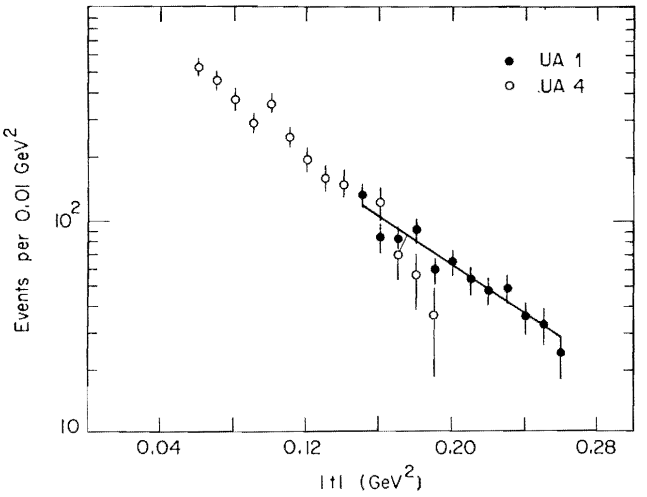

Figure 4. Elastic Scattering Results (UA1, UA4)

a simultaneous measurement of low-t elastic scattering and the total inelastic rate. Using the optical theorem one can write the differential elastic rate as

$$\frac{dN_{el}}{dt} = L\frac{\sigma_t(1+\rho^2)}{16\pi(\hbar c)^2}\exp(bt)$$

where ρ is the ratio of the real to imaginary parts of the forward scattering amplitude and L is the luminosity. Furthermore

$$N_{el}+N_{inel}=L\sigma_t$$

where N_{el} and N_{inel} are the total elastic and inelastic rates. Combining the two expressions and extrapolating the elastic scattering to $t=0$ allows the luminosity to be eliminated giving

$$\sigma_t=\frac{16\pi(\hbar c)^2}{1+\rho^2}\frac{\left[\frac{dN_{el}}{dt}\right]_{t=0}}{N_{el}+N_{inel}}$$

Figure 5 shows the UA4 result [14] of 66 ± 7 mb compared to lower energy measurements. The rise of the total cross section agrees with dispersion relation predictions [15] (see curves).

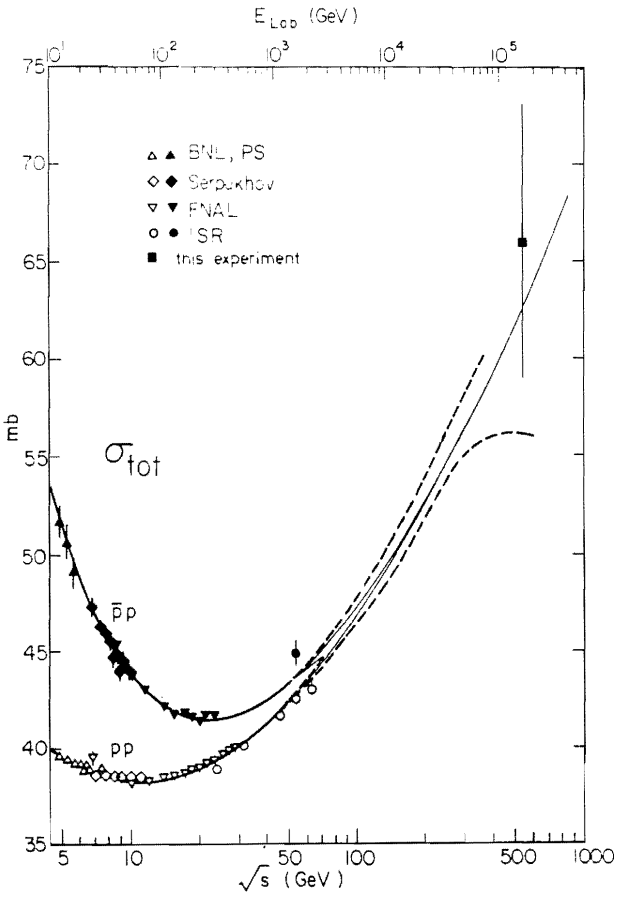

Figure 5. The Total Cross Section for $p\bar{p}$ and pp. The Lines are a Dispersion Relation Fit [15] (UA4)

4. MINIMUM BIAS PHYSICS

4.1. Pseudo-Rapidity Density Distributions

Charged particle multiplicities as a function of pseudo-rapidity $\eta=-\ln(\tan\theta/2)$ have been studied by UA5 [16,17] and UA1 [18] using zero-field data. Excellent agreement is found. In addition UA5 has studied photon multiplicities by detecting γ-conversions in the beam vacuum pipe and the lead-glass plates. Figure 6 shows the UA5 results and includes ISR measurements [19] at $\sqrt{s}=53$ GeV for comparison. Simple Feynman scaling [20] says that the pseudo-rapidity density $dn/d\eta=1/\sigma_{inel}\ d\sigma/d\eta$ should be constant, independent of s. Because the range of rapidity available increases as $\ln s$ the average multiplicity of the event would then increase as $\ln s$. It is already known from the ISR [21] that the average central rapidity density $\left[\frac{dn}{d\eta}\right]_{\eta=0}$ increases by 40% from $\sqrt{s}=23$ to 63 GeV violating Feynman scaling. A continued $\ln s$ dependence is observed in moving to collider energy $\sqrt{s}=540$ GeV (Figure 7). As a consequence the average total charged multiplicity increase to $\langle n_{ch}\rangle=26.5\pm1$ [17] requires an $(\ln s)^2$ term to account for its energy dependence. However the width of the pseudo-rapidity density distribution has grown by only 2 units from ISR to collider compared to the 4.6 units available kinematically. Furthermore, a cylindrical phase space description with $\langle p_t\rangle=0.35$ GeV/c that describes the ISR data (solid curves) fails to account for the collider results.

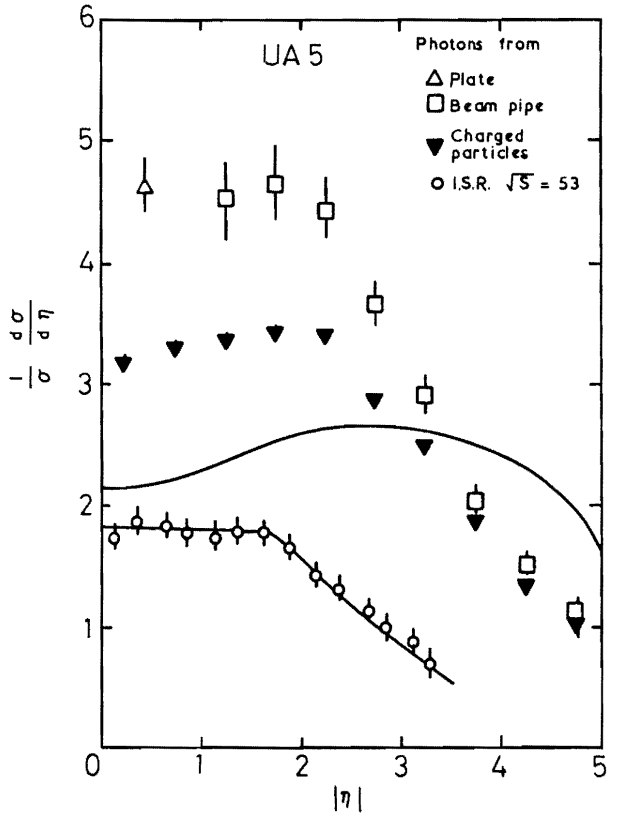

Figure 6. Pseudo-rapidity Density Distributions for Charged Hadrons and Photons (UA5)

One explanation could be that the mean particle transverse momentum has increased so limiting the rapidity and UA5 [16] were able to obtain agreement with the collider results for $\langle p_t \rangle = 0.50$ GeV/c. UA1 measurements [25] (see later), however, give $\langle p_t \rangle = 0.42$ GeV/c so this may not be the whole reason.

There is an excess of photons compared to charged particles (Figure 6). If all particles were pions the number of photons from π^0 decays would equal the number of $\pi^{\pm}$ on average. The excess can be accounted for by a 32% contribution from η-decays when allowance is also made for strange particles and protons [17]. UA2 [22] have used their lead-glass array to study photon production for $|\eta| < 0.7$ and find $\eta/\pi^0 = 0.55$ consistent with ISR measurements, but for $p_t > 1.5$ GeV/c. The UA5 measurements [17] show that $\langle n_\gamma \rangle$ rises linearly with the number of charged particles up to the highest multiplicity studied (~ 80).

4.2. Multiplicity Distributions

If particles were produced randomly and independently their multiplicity might be expected to obey a Poisson distribution $P_n = e^{-\langle n \rangle} \langle n \rangle^n / n!$ which would become relatively narrower (as $\sim 1/\sqrt{n}$) as the energy and hence multiplicity increased. Koba, Olesen, and Nielsen [23] showed, starting from Feynman scaling, that on the contrary the shape of the distribution should tend to become constant as $s \to \infty$ (KNO scaling). Thus if $P_n \langle n \rangle$ is plotted against $z = n/\langle n \rangle$, where P_n is the probability of observing a multiplicity n, the distributions at different energies should coincide at sufficiently high energy. The collider results [16–18] show excellent agreement with KNO scaling when compared to ISR measurements [21] both for a restricted rapidity range (Figure 8) and for the full rapidity plateau in spite of the substantial violation of Feynman scaling. At $\sqrt{s} = 540$ GeV the distribution is much wider than a Poisson distribution and in good agreement with an independent cluster model [24] derived by de Groot to account for ISR data [21] (Figure 9).

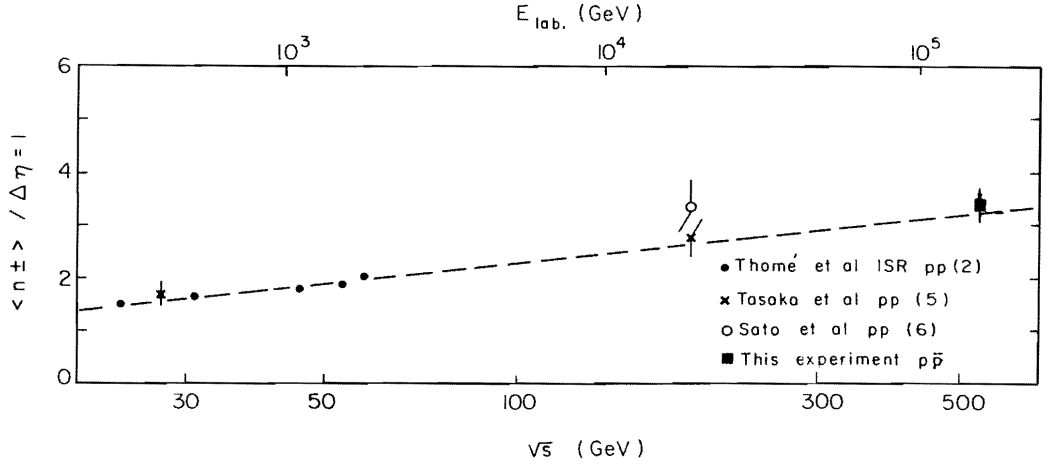

Figure 7. Average Multiplicity per Unit of Rapidity at $\eta = 0$ as a Function of Energy (UA1)

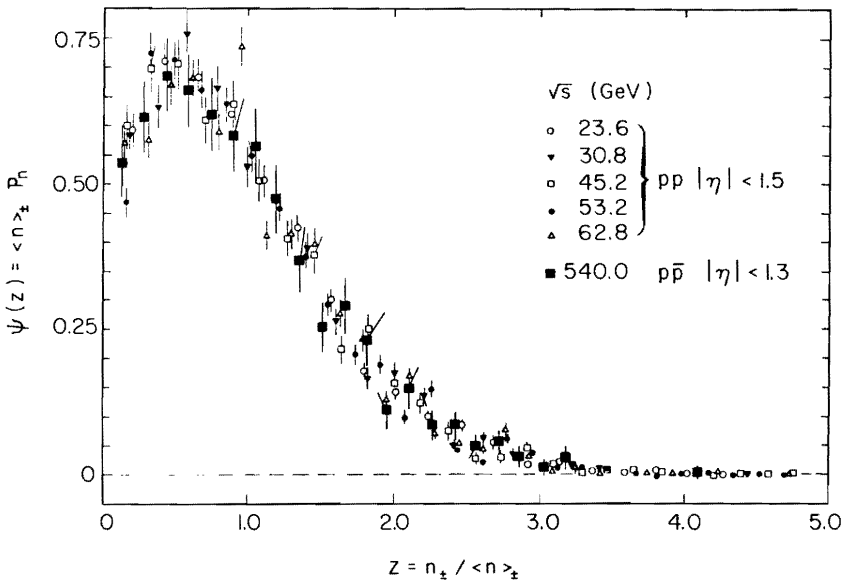

Figure 8. Multiplicity Distributions for Restricted η Plotted in KNO Variables (UA1)

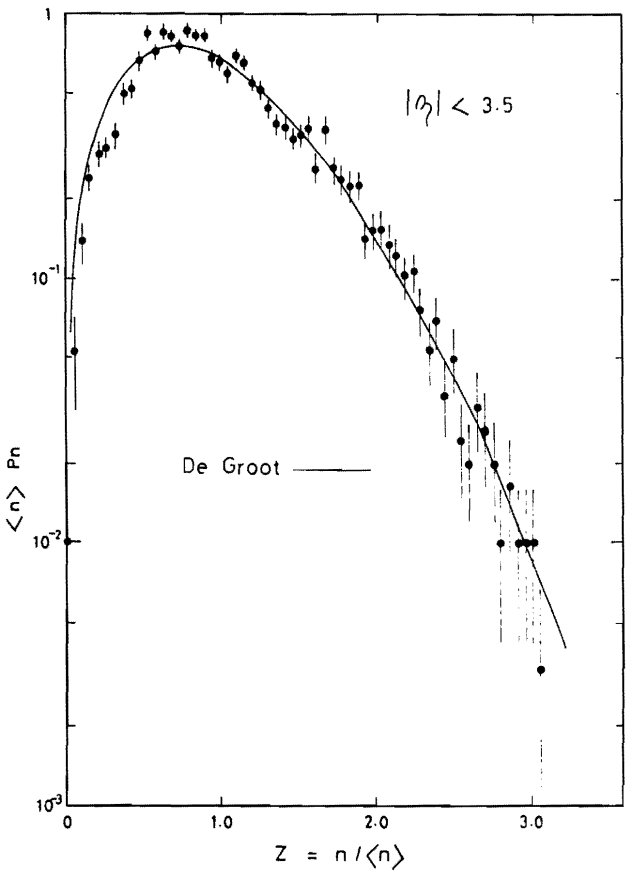

Figure 9. Multiplicity Distribution for the Full Plateau Region Compared to the Independent Cluster Model of de Groot [24] (UA1)

4.3. p_t—distributions and Particle Ratios

The transverse momentum spectrum for unidentified charged hadrons observed by UA1 is given in Figure 10 for three different bands of multiplicity averaged over the interval $|y|<2.5$ [25]. The three spectra have been normalized to the full inclusive cross section at $p_t=0$. Even at rather low p_t values the spectrum becomes flatter with increasing multiplicity, a result already suggested by cosmic ray experiments [26]. The average transverse momentum $\langle p_t \rangle$ increases with multiplicity (Figure 11) and becomes constant at very high multiplicity. This may be a saturation effect. The points without error bars give $\langle p_t \rangle$ averaged over all multiplicities at FNAL, ISR, and the collider. The fact that the lower energy points tend to lie on the same curve suggests that $\langle p_t \rangle$ may be related to multiplicity in some general way.

The UA2 group [27] has measured the p_t spectrum of pions, $\pi^{\pm}$ being identified by time of flight ($p_t<1.5$GeV/c) and π^0 by reconstruction from their decay. Good agreement is found (Figure 12) between the two. For $p_t<1.2$GeV/c charged kaons and protons have been identified and the ratios K/π and p/π are independent of the transverse mass (Figure 13).

UA5 have identified K^0 and Λ^0 from their decays into charged particles. Their p_t distributions (Figure 14) are less steep than for pions with mean transverse momenta of 0.70 ± 0.12 and 0.67 ± 0.20GeV/c for

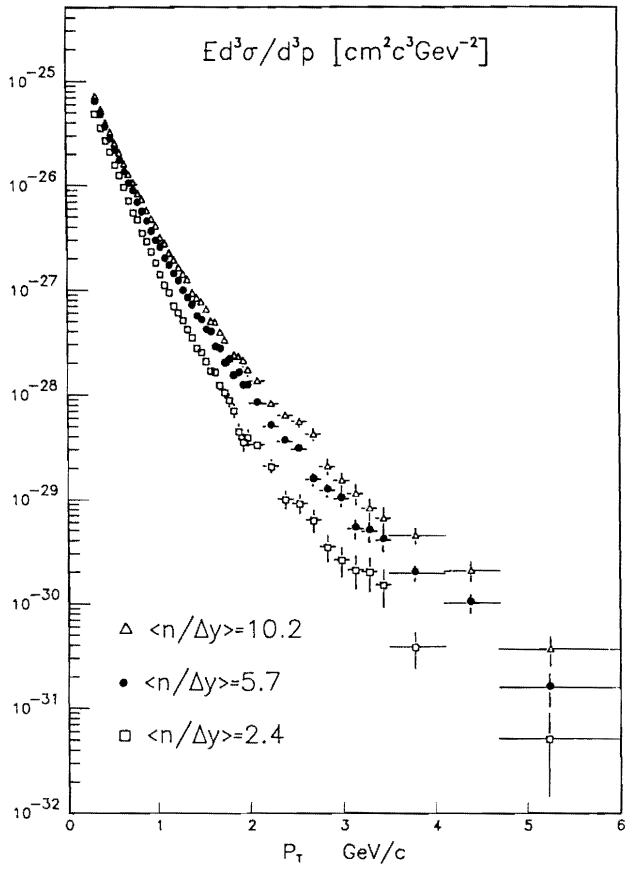

Figure 10. p_t *Distributions for Various Multiplicity Bands (UA1)*

kaons and lambdas respectively. The multiplicity of the neutral kaons $(K^0+\overline{K^0})$ is 2.0 ± 0.4 per inelastic event while for $(\Lambda^0+\overline{\Lambda^0})$ it is 0.35 ± 0.10. The ratio of $(K^0+\overline{K^0})/\pi^{\pm}$ is $11\pm2\%$ showing a rise from lower energies (Figure 15) possibly due to increasing heavy flavor production. The apparently higher K/π ratio in Figure 13 is a consequence of the different p_t distributions for πs and Ks. These results also indicate a rise from the ISR energy range.

4.4. Transverse Energy Distributions

The central calorimeters of the UA1 experiment [29] have been used to study the transverse energy distribution for $|\eta|<3.0$. As all the particles deposit their energy in the calorimeters the total transverse energy E_T should be simply related to the multiplicity of the event and the p_t carried by each particle within the selected η-region. It is found that E_T rises almost linearly with observed multiplicity (Figure 16(a)) showing that selecting high E_T preferentially selects large multiplicity. Similar observations were made in the NA5 experiment at CERN [30]. A high E_T trigger is the natural way to search for high p_t jets in an unbiased way so these high multiplicity events are a background at least at the triggering level. Figure 16(b) shows the average E_T per charged particle. The curve is a Monte Carlo prediction, allowing for neutrals, and using the observed multiplicity distribution, but taking the single particle p_t distribution to be independent of multiplicity. The fact that the points rise above the curve for increasing multiplicity confirms that $\langle p_t \rangle$ is a function of multiplicity.

5. LARGE TRANSVERSE MOMENTUM SCATTERING AND JETS

5.1. Single Particle p_t Spectra

Particles produced by 'soft' processes have mainly been discussed so far. They are expected to have a Gaussian p_t dependence $dN/dp_t^2 \propto \exp(-bp_t^2)$. 'Hard'

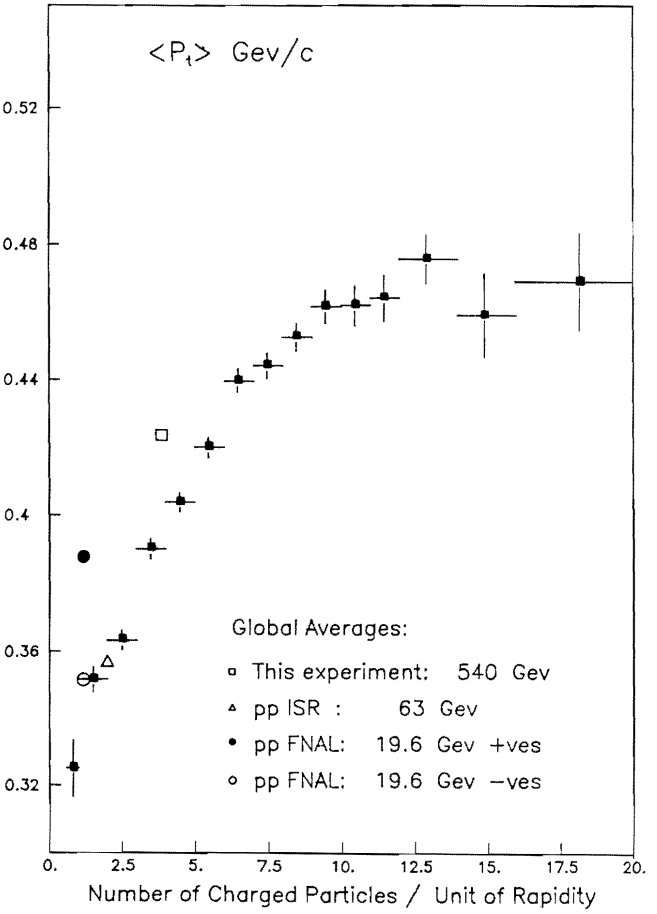

Figure 11. $\langle p_t \rangle$ *as a Function of Rapidity Density (UA1)*

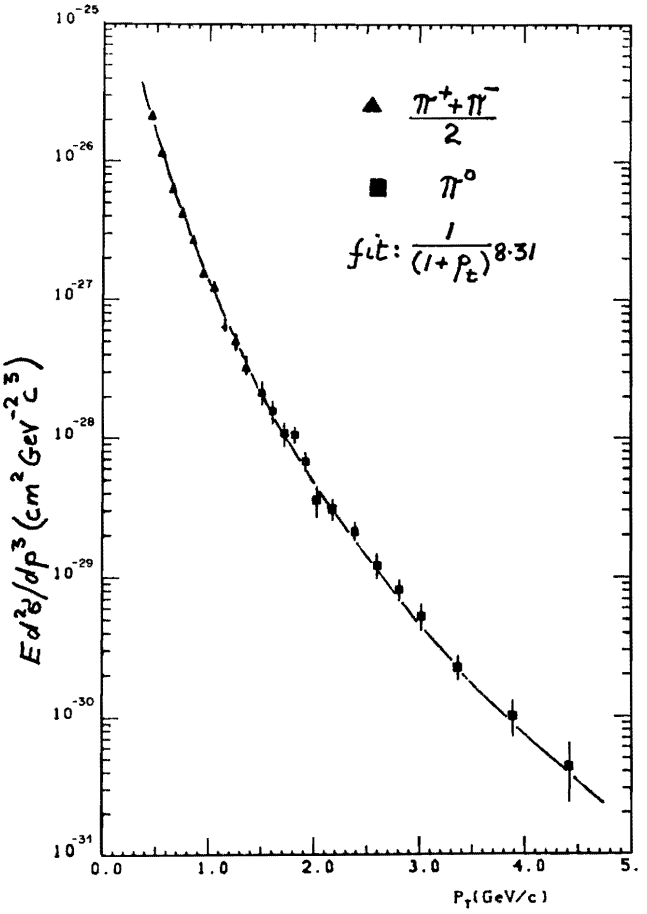

Figure 12. p_t *Distribution for Identified Pions (UA2)*

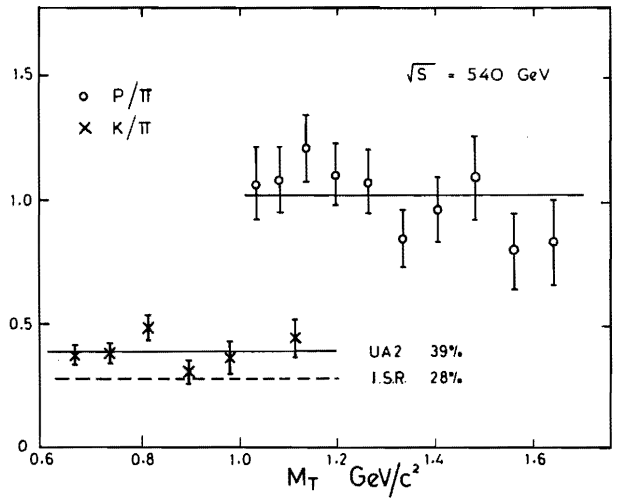

Figure 13. K/π *and* p/π *Ratios as a Function of Transverse Mass* $m_T = p_t^2 + m^2$ *(UA2)*

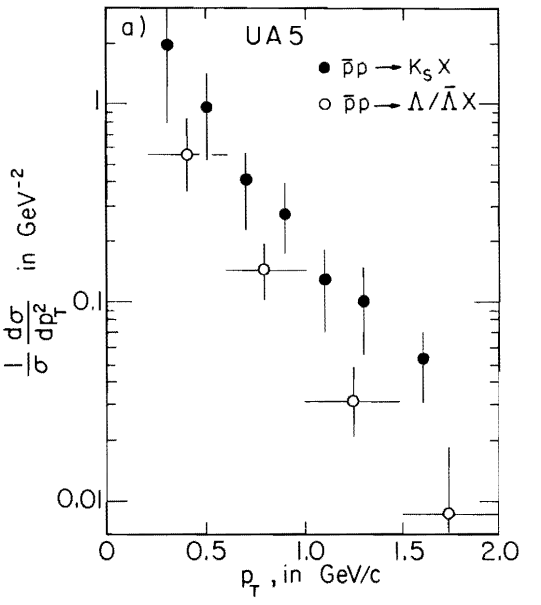

Figure 14. p_t *Distributions for* K^0 *and* Λ^0 *(UA5)*

processes, on the other hand, in which point-like partons scatter are naively expected to behave as $dN/dp_t^2 \propto p_t^{-4}$, in analogy with Rutherford scattering. Such a power-law behavior should dominate the scattering at sufficiently high p_t because of its less steep p_t dependence. Parton scattering gives rise to jets in the final state (fragmentation) but the individual particles within a jet should reflect the parents power-law behavior. QCD and parton structure effects modify this simple argument but the basic point remains true.

The invariant cross section for unidentified charged hadrons as a function of transverse momentum [25] is given in Figure 17 for $|y|<2.5$. The distribution is considerably flatter than that at the ISR [31] at

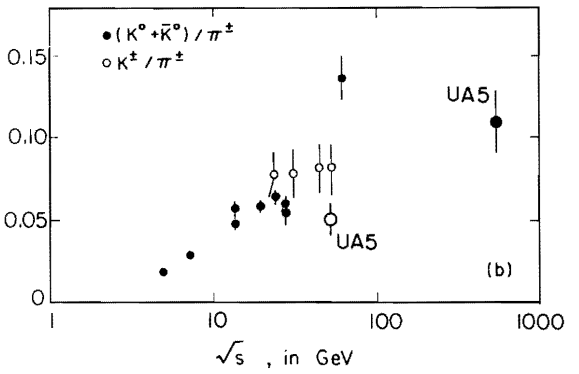

Figure 15. The K/π *Ratio as a Function of Energy (UA5)*

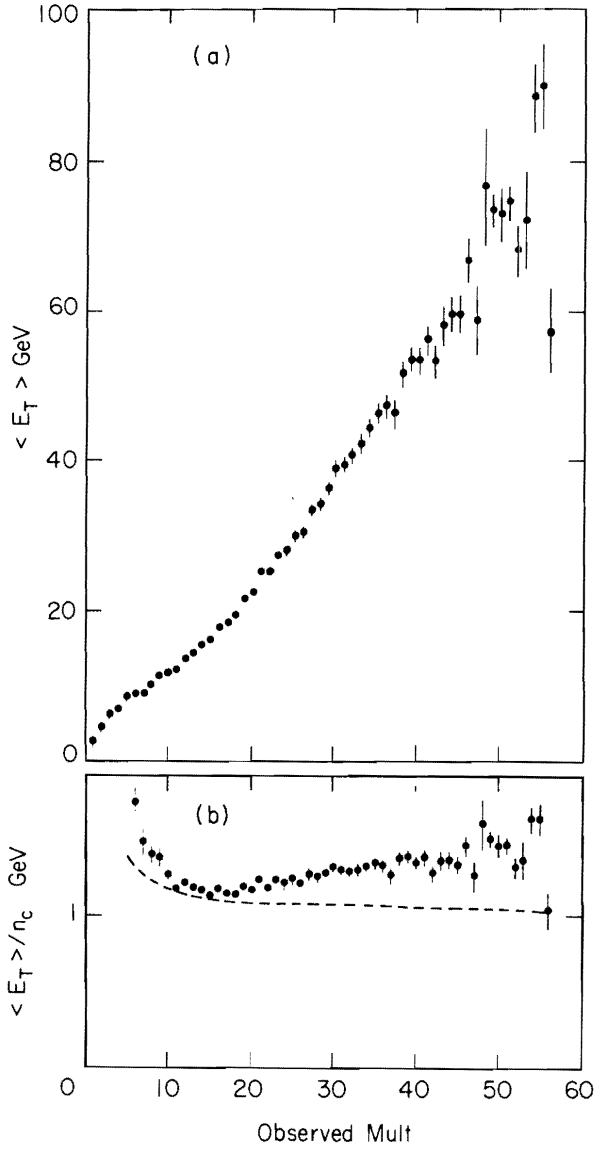

Figure 16. (*a*) *Total Transverse Energy for* $|\eta| < 3.0$ *versus Multiplicity.*

(*b*) *Average* E_T *per Charged Particle versus Multiplicity* (*See Text*) (*UA1*)

$\sqrt{s}=63$ GeV exceeding it by three orders of magnitude at $p_t=10$ GeV/c. The QCD calculations of Odorico [32], which include the effect of gluon radiation of the initial and final state partons, are shown in the figure and agree well with the data. The p_t-dependence for the collider data is close to p_t^{-8}, very different from the naive prediction but nevertheless expected. It is a consequence of the sharply peaked parton distributions at low x in the colliding hadrons and scaling violations in the structure and fragmentation functions.

Measurements from the UA1 end-cap electromagnetic calorimeters [33] for $1.6<|y|<2.5$ are included in Figure 17 (a further point at 12 GeV/c is not shown). These include π^0, η^0 and γ and agree well in spite of the different rapidity range and particle composition.

5.2. Evidence for Clustering

Both UA1 and UA2 have observed clusters of particles with high p_t indicating jet production. In UA1 [34] a trigger particle measured in the central drift chambers was defined as that having the largest p_t and at least 4 GeV/c. The distributions of the rapidity difference, Δy, and azimuthal angle difference, $\Delta\phi$, of all other particles relative to the trigger particle are plotted in Figure 18. The Δy distributions are plotted separately for the hemispheres centered around the trigger particle ('towards') and opposite to it ('away'). A correlation in y which becomes sharper with increasing secondary particle p_t is seen on the

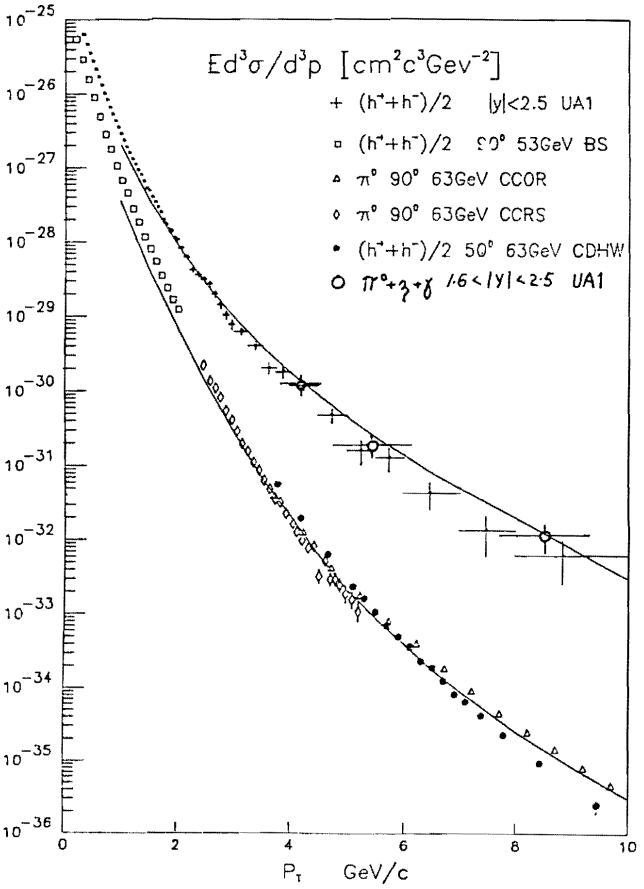

Figure 17. The invariant cross sections as a function of transverse momentum at ISR energies and the collider $\sqrt{s}=540$ *GeV* (*UA1*)

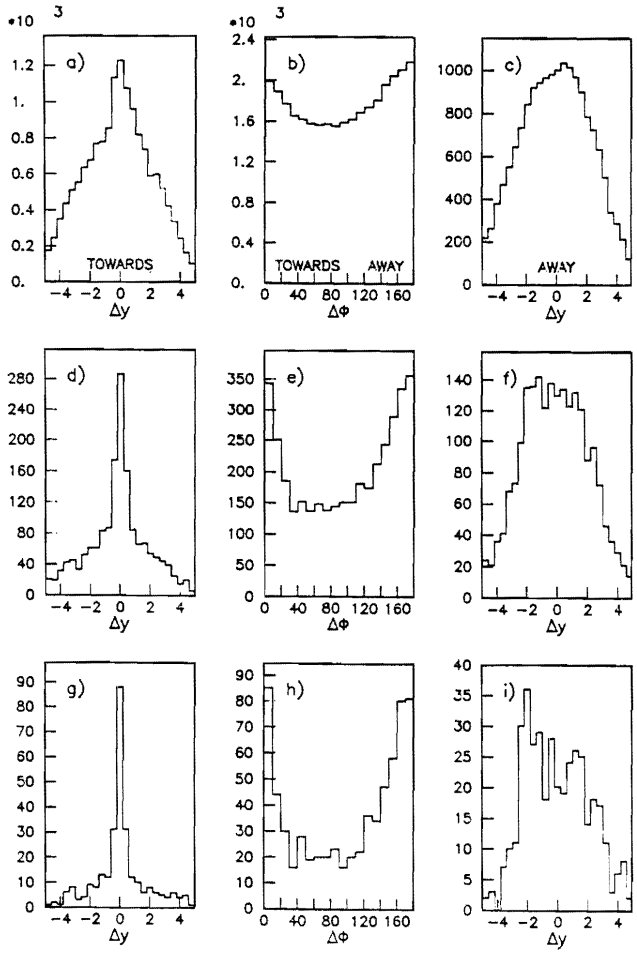

Figure 18. Rapidity Differences between Secondaries and a Trigger Particle of $p_t > 4GeV/c$ *in (a) the Towards and (c) the Away Hemisheres; (b) Azimuthal Difference. The Three Rows are for Secondary* $p_t > 0$, *1, and 2GeV/c (UA1)*

'towards' side but not on the 'away' side. Simultaneously, there is a peaking for $\Delta\phi = 0°$ and $\Delta\phi = 180°$, i.e. opposite azimuths. These features are expected for jets produced by colliding partons. The trigger particle defines the jet-axis reasonably well and the large p_t secondaries cluster around it because of their limited transverse momenta with respect to the parton direction. The away-side jet is expected to be coplanar to balance p_t, explaining the ϕ correlation, but cannot be predicted in y because of the lack of knowledge of the colliding parton momenta in the incident hadrons.

Both UA1 and UA2 have used their calorimeters to look for localized depositions of energy. Clusters of adjacent cells are defined using suitable algorithms and it is found that the fraction of the total transverse energy that is deposited into one or more clusters increases as ΣE_T is raised reaching levels of 50% in a single cluster for $\Sigma E_T \sim 100\,\text{GeV}$ and $|\eta| < 1.0$ in UA2 [35]. Comparable figures are found in UA1 showing that for such high ΣE_Ts the fraction of jet-like events is indeed large. Many examples of spectacular events have been observed. Figure 19 shows a two-jet event from UA2 having a jet-jet mass of $\simeq 140\,\text{GeV}/c^2$ and Figure 20 a three-jet event from UA1 with a mass of $\sim 90\,\text{GeV}/c^2$.

5.3. Jet Cross Sections

UA1 and UA2 have determined jet cross sections and are broadly in agreement although the UA1 values are somewhat higher than those of UA2. Taken together they agree well with QCD predictions, a very satisfactory result at the present stage of study. Figure 21 shows the inclusive jet production cross section from UA2 [35]. The solid curve is the QCD calculation of Horgan and Jacob [36] using 0.5 GeV for the strong coupling parameter Λ. The dashed line is for $\Lambda = 0.15\,\text{GeV}$. Figure 22 shows the corresponding results for UA1 [37] with curves from reference [36] and from Furmanski and Kowalski. At these values of the jet E_t gluon–gluon scattering dominates [36] because low parton x-values are involved. Consequently the collider offers the possibility of studying gluon fragmentation functions. In contrast, at the ISR quark jets are more important because of the larger x-values needed for the partons to produce high p_t collisions. Figure 21 shows results for jet production at the ISR [38]. They are well described by the same QCD calculations.

6. SEARCH FOR CENTAUROS AND FREE QUARKS

Centauro events, seen in cosmic rays [39], are half a dozen high energy events characterized by a high multiplicity of hadrons and a multiplicity of electromagnetically showering particles consistent with zero. The hadrons have an abnormally high $\langle p_t \rangle$ ($\sim 1\,\text{GeV}/c$).

UA1 has used the energy deposited in the first four radiation lengths of the electromagnetic calorimeters as a measure of electromagnetic energy and compared this with the hadronic energy to look for abnormal sharing [40]. No evidence for any clustering of events with unusual properties is seen in a sample of 48,000 even after selecting those with high p_t and multiplicity. UA5 has seen no candidates in a sample of 1860

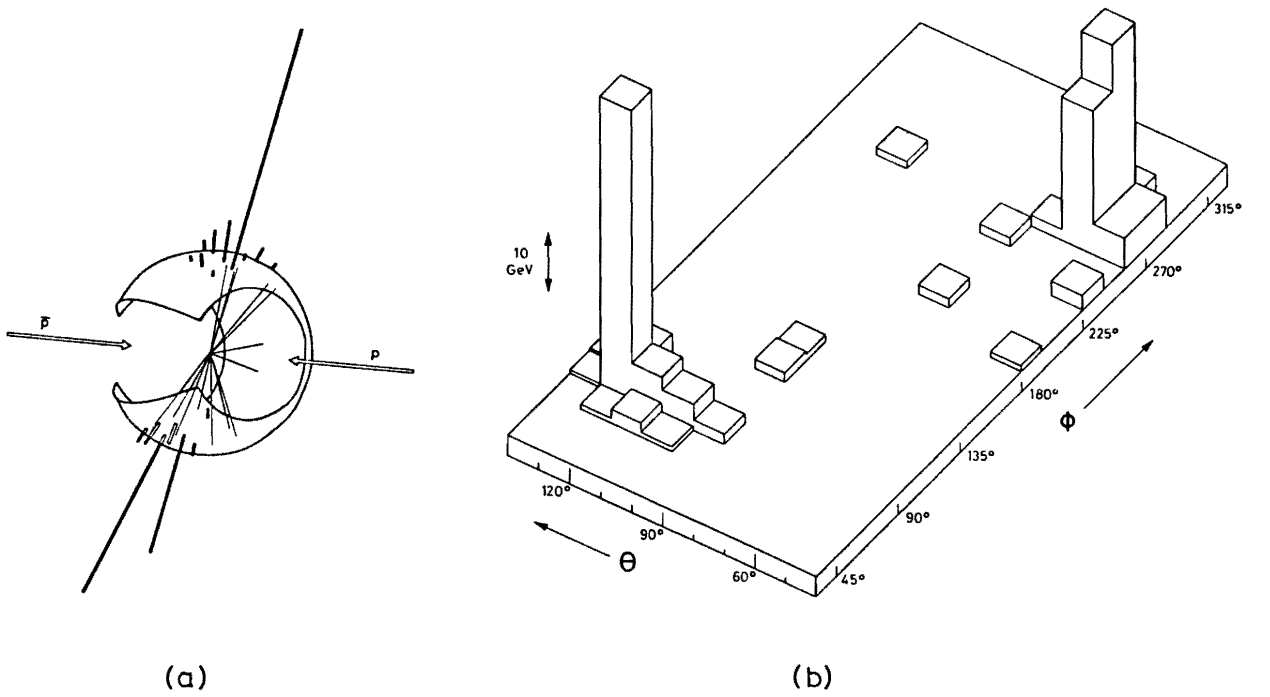

Figure 19. Configuration of an Event in the UA2 Apparatus Showing (a) Charged Tracks (Inside) and Calorimeter Cell Energies, (b) the Cell Energy Distributions as a Function of Polar Angle θ and Azimuth φ.

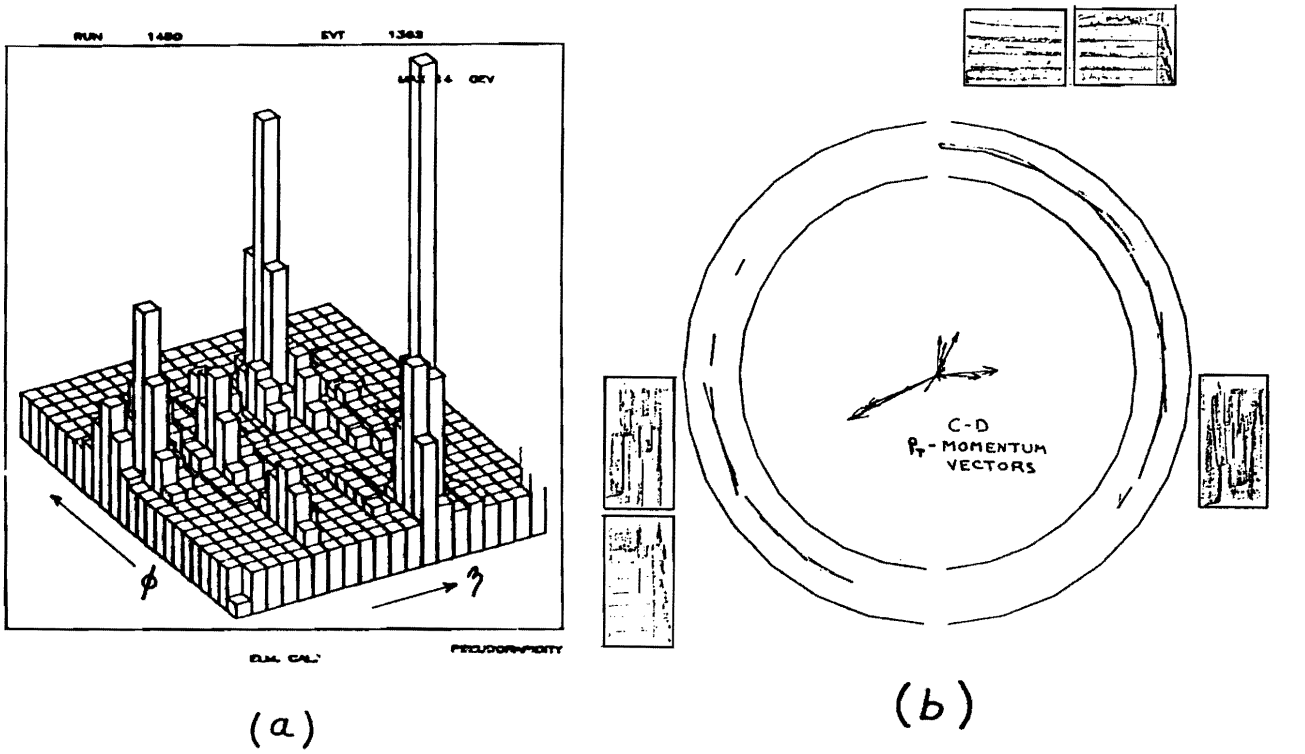

Figure 20. A Three-jet Event in the UAI Apparatus Showing (a) an η,φ Plot of Calorimeter Energy and (b) Corresponding p_t Vectors in the Central Track Detector.

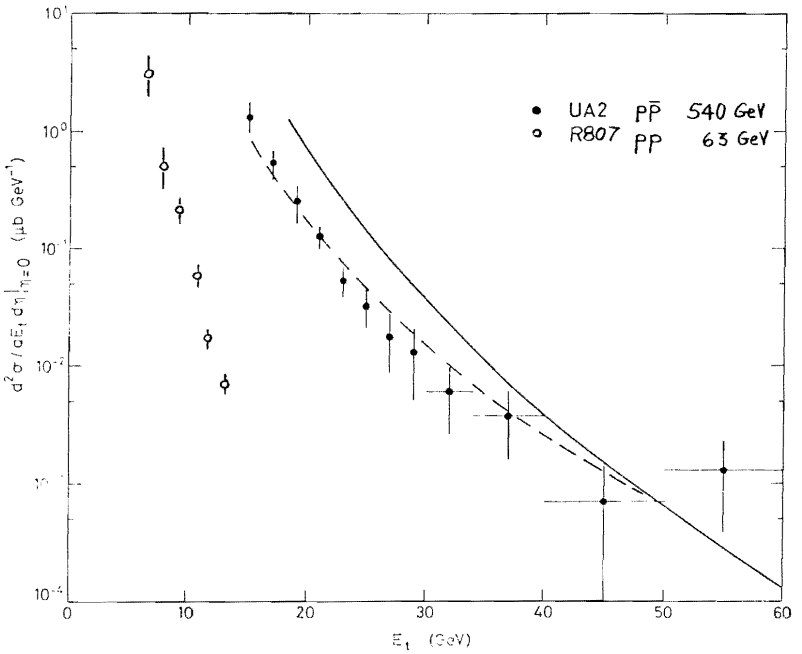

Figure 21. Inclusive Jet Production Cross Sections at the Collider and ISR. The Solid Line is a QCD Calculation of Horgan and Jacob [36] with A=0.5 GeV. The Dashed Line is for A=0.15 GeV

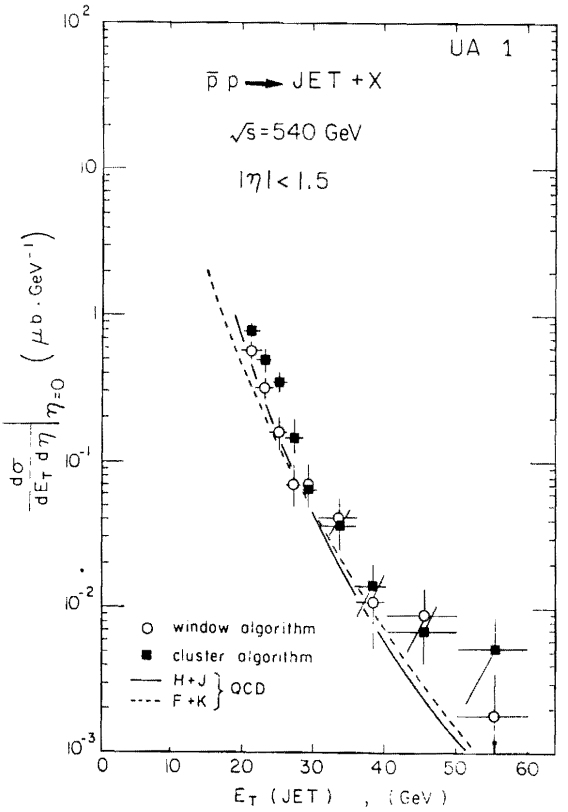

Figure 22. Inclusive Jet Cross Sections from the UA1 Experiment Obtained by Two Methods. The Solid Line is the QCD Calculation of Reference [36]

events [17]. However, the collider has only one-third of the center of mass energy at which Centauros have been reported [39].

.UA2 has searched for fractionally charged particles [45] using their ionization in a set of scintillation counters. For light quarks ($m \sim 0$) they quote a 90% confidence level limit of $< 2.2 \times 10^{-4}$, relative to singly charged particles, for either $Q = 1/3$ or $Q = 2/3$.

7. OBSERVATION OF THE W

The outstanding result so far obtained at the collider is the observation of the weak intermediate boson, W, the carrier of the electroweak force. From the 1982 data UA1 has five events and UA2 four events that have the characteristics expected of $W \rightarrow e\nu$. If the W decays perpendicular to the beam in its rest frame then the electron and the neutrino will each carry a transverse momentum equal to half its mass (i.e. about 40 GeV/c). Over quite a large part of the solid angle for the decay products the p_t does not change very much so one expects a Jacobian peak at $m_W/2$. Figure 23 shows the UA1 result [41] for events in which an electron candidate, defined as a charged particle giving up its energy in the electromagnetic calorimeters and having a matching central detector

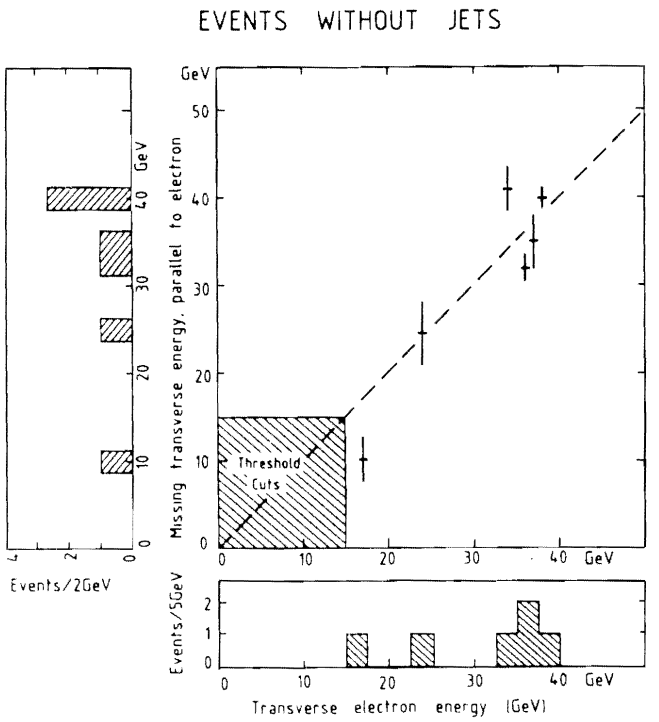

Figure 23. Transverse Energy for Isolated Electrons Plotted against the Missing Transverse Energy in the UA1 Experiment. Events from W Decay Should Lie on the Dashed Line

momentum measurement, is accompanied by 'missing transverse energy' corresponding to an unseen neutrino. Both electron and neutrino have the expected peaking towards 40 GeV and are related in the way that would be expected for W decay. The events were obtained from a total of about 10^9 collisions, a rate consistent with the expected cross section [42]. The integrated luminosity was $2 \times 10^{34}\,\mathrm{cm}^{-2}$. Figure 24 shows the energy deposited in the electromagnetic calorimeter of UA2 [43] for one of the events. The W-mass estimates from UA1 and UA2 are respectively $81 \pm 5\,\mathrm{GeV}/c^2$ and $80^{+10}_{-6}\,\mathrm{GeV}/c^2$ consistent with the expectation from the Weinberg–Salam theory of $82 \pm 2.4\,\mathrm{GeV}/c^2$ [44].

8. FUTURE PROSPECTS

With an anticipated increase in integrated luminosity of a factor 5 in 1983 observation of the Z^0 particle is expected if the Weinberg–Salam theory is correct. Now that backgrounds for W production have been seen to be small, higher statistics will permit more detailed tests of the theory such as the decay asymmetry. In the longer term improvements to the

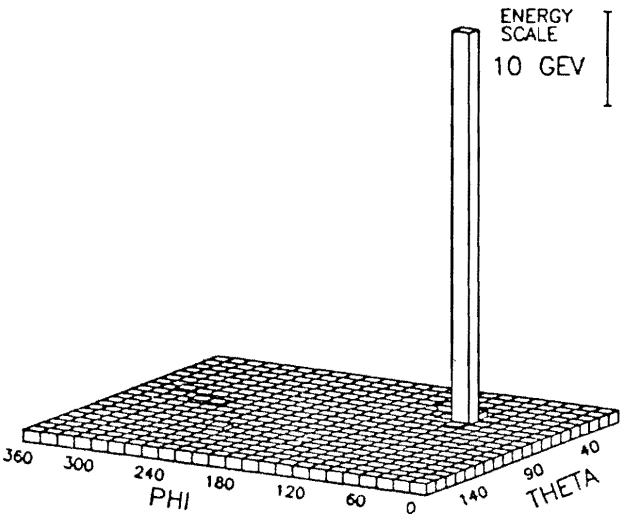

Figure 24. Energy Deposition in the UA2 Electromagnetic Calorimeters for a W Event

accumulation rate of antiprotons by adding a collector ring could produce a tenfold increase in luminosity allowing even more refined studies including the top-quark and possibly other new particles expected theoretically such as the Higgs meson.

Note added in proof

Four examples of the Z^0 decaying to e^+e^- and one to $\mu^+\mu^-$ have now been reported from the UA1 experiment (G. Arnison and others, *Physics Letters*, **126B** (1983), p. 398). The mass, $95.2 \pm 2.5\,\mathrm{GeV}/c^2$, is consistent with the standard electroweak model.

REFERENCES

[1] C. Rubbia, P. McIntyre, and D. Cline, *Proceedings of the International Neutrino Conference*, Aachen, 1976 (Vieweg, Branschweig, 1977), p. 683.

[2] G. Carron and others, *Physics Letters*, **77B** (1978), p. 363.

[3] S. van der Meer, 'Proton–Antiproton Colliding Beam Facility', CERN/SPC/423 (1978).

[4] B. Autin and others, 'Design Study of a Proton–Antiproton Colliding Beam Facility', CERN/PS/AA 78–3.

[5] K. Akesson and others, *Physics Letters*, **108B** (1982), p. 58.
K. Alpgard and others, *Physics Letters*, **112B** (1982), p. 183.
D. Favart and others, *Physical Review Letters*, **47** (1981), p. 1191.
G. Carboni and others, *Physics Letters*, **113B** (1982), p. 87.
A. Breakstone and others, *Physics Letters*, **114B** (1982), p. 383.

[6] Aachen–Annecy (LAPP)–Birmingham–CERN–London (Queen Mary College)–Paris (College de

France)–Riverside–Rutherford–Saclay (CEN)–Vienna Collaboration (UA1), CERN/SPSC/78-06/P92.
M. Barranco Luque and others, *Nuclear Instruments and Methods*, **176** (1980), p. 175.
M. Calvetti and others, *Nuclear Instruments and Methods*, **176** (1980), p. 255.
K Eggert and others, *Nuclear Instruments and Methods*, **176** (1980), pp. 217 and 223.
A. Astbury, *Physica Scripta*, **23** (1981), p. 397.

[7] Bonn, CERN, Copenhagen, Orsay, Pavia, Saclay collaboration (UA2), CERN/SPSC/78-08/P93, CERN/SPSC/78-54, and contribution *International Conference on Instrumentation for LEP*, Uppsala, 15–20 June (1980).

[8] Annecy(LAPP)–CERN collaboration (UA3), CERN/SPSC/78-15/P96.

[9] Amsterdam–CERN–Genova–Napoli–Pisa collaboration (UA4), CERN/SPSC/78-105/P114.

[10] Bonn–Brussels–Cambridge–CERN–Stockholm collaboration (UA5), CERN/SPSC/78-38/P101, and *Physica Scripta*, **23** (1981), p. 642.

[11] R. Battiston and others, *Physics Letters*, **115B** (1982), p. 333.

[12] G. Arnison and others, *Physics Letters*, **121B** (1983), p. 77.

[13] J. P. Burq and others, *Physics Letters*, **109B** (1982), p. 124.

[14] R. Battiston and others, *Physics Letters*, **117B** (1982), p. 126.

[15] U. Amaldi and others, *Physics Letters*, **66B** (1977), p. 390.

[16] K. Alpgard and others, *Physics Letters*, **107B** (1981), p. 310. ibid. p. 315.

[17] K. Alpgard and others, *Physics Letters*, **115B** (1981), p. 71.

[18] G. Arnison and others, *Physics Letters*, **107B** (1981), p. 320, and **123B** (1983), 108.

[19] K. Alpgard and others, *Physics Letters*, **112B** (1982), p. 183.

[20] R. P. Feynman, *Physics Review Letters*, **23** (1969), p. 1415.

[21] W. Thomé and others, *Nuclear Physics*, **B129** (1977), p. 365.

[22] P. Jenni, CERN-EP/82-107 (see also [27]).

[23] Z. Koba, H. B. Nielsen, and P. Oleson, *Nuclear Physics*, **B40** (1972), p. 317.

[24] E. H. de Groot, *Physics Letters*, **57B** (1975), p. 159.

[25] G. Arnison and others, *Physics Letters*, **118B** (1982), p. 167.

[26] G. M. G. Lattes and others, *Physics Reports*, **65** (1980).

[27] M. Banner and others, *Physics Letters*, **115B** (1982), p. 59 and **122B** (1983), p. 322.

[28] K. Alpgard and others, *Physics Letters*, **115B** (1982), p. 65.

[29] G. Arnison and others, CERN-EP/82-122.

[30] K. Pretzl, paper presented at the *Forward Collider Workshop*, Madison (1981).

[31] B. Alper and others, *Nuclear Physics*, **B100** (1975), p. 237.
A. L. S. Angelis and others, *Physics Letters*, **79B** (1978), p. 505.
F. W. Busser and others., *Nuclear Physics*, **B106** (1976), p. 1.
D. Drijard and others, CERN-EP/82-70. Submitted to *Nuclear Physics* **B**.

[32] R. Odorico, Paper presented at the *XXI International Conference on High Energy Physics*, Paris, 26–31 July (1982).

[33] G. Arnison and others, CERN-EP/82-120.

[34] G. Arnison and others, *Physics Letters*, **118B** (1982), p. 173.

[35] M. Banner and others, *Physics Letters*, **118B** (1982), p. 203.

[36] R. Horgan and M. Jacob, *Nuclear Physics*, **B179** (1981), p. 441.

[37] G. Arnison and others, *Physics Letters*, **123B** (1983), p. 115.

[38] M. G. Albrow and others, *Nuclear Physics*, **B160** (1979), p. 1.
A. L. S. Angelis and others, *Physica Scripta*, **19** (1979), p. 116.
A. C. Clark and others, *Nuclear Physics*, **B160** (1979), p. 397.
D. Drijard and others, *Nuclear Physics*, **B166** (1980), p. 233.
see also reviews by:
K. Hansen and P. Hoyer, *Physica Scripta*, **19** (1979).
P. Darriulat, *Annual Review of Nuclear Particle Science*, **30** (1980), p. 159.

[39] M. Ballester and others, *Proceedings of the 17th International Cosmic Ray Conference* (Paris, 1981) (CEA, Saclay, 1981), **11**, p. 159.
see also [26].

[40] G. Arnison and others, *Physics Letters*, **122B** (1983), p. 189.

[41] G. Arnison and others, *Physics Letters*, **122B** (1983), p. 103.

[42] R. F. Peierls, T. Trueman, and L. L. Wang, *Physical Review*, **D16** (1977), p. 1397.

[43] M. Banner and others, *Physics Letters*, **122B** (1983), p. 476.

[44] C. H. Llewellyn Smith and J. A. Wheater, *Physics Letters*, **105B** (1981), p. 486.

[45] M. Banner and others, *Physics Letters*, **121B** (1983), p. 167.

Paper Received 29 May 1983.